CONF-860316--14

UCRL--93864

DE87 009594

TRANSITION RADIATION AS A COHERENT SOFT X-RAY SOURCE

Michael J. Moran
D. B. Dahling

M. A. Piestrup, Adelphi Technologies
B. L. Berman, George Washington University
J. O. Kephart, Stanford University

Presented at: 3rd Topical Meeting on
Short Wavelength Radiation: Generation & Application

Monterey, CA
March 24-26, 1986

Transition Radiation as a Coherent Soft X-ray Source

M.J. Moran, B.A. Dahling, M.A. Piestrup
Lawrence Livermore National Laboratory, University of California
Livermore, CA 94550

and

B.L. Berman
Department of Physics, George Washington University
Washington, D.C. 20052

and

J.O. Kephart
Department of Electrical Engineering, Stanford University
Stanford, CA 94305

A series of experiments using 54 Mev electrons to irradiate thin foil targets has demonstrated the spatially coherent nature of soft x-ray transition radiation.

An ongoing series of experiments at the Lawrence Livermore National Laboratory electron positron linear accelerator has studied transiton radiation produced by 25- and 54-Mev electrons traversing targets consisting of thin low-Z foils. Our results have been consistent with theoretical predictions of the absolute intensity and angular and spectral distributions of photon emissions in the soft x-ray energy range.[1,2] Energy-integrated measurements of the angular distribution have demonstrated that these x-rays are spatially coherent with respect to the two surfaces of individual foils and also with respect to all of the foils in multiple-foil targets. Energy-resolved measurements of the angular distributions have further demonstrated the transition radiation spatial coherence and point the way to application of these experiments to the study of x-ray properties of materials and to the development of new kinds of coherent photon sources.

Figure 1 shows the experimental arrangement that was used for the first series of measurements. Here, a flow-type proportional counter using a mixture of 90% neon and 10% isobutane was remotely scanned across the beam line to measure the angular distribution, with 1 mrad resolution, of x rays with energies from 300 eV to about 6 keV. The targets consisted of from one to twenty foils, approximately 1 μm-thick, of beryllium, carbon, mylar, magnesium, aluminum, silicon, and titanium. After traversing the target, the electron beam was deflected into a dump-hole in the floor where a scintillation detector was used to monitor the beam current. Backgrounds were due mostly to bremsstrahlung, were generally small compared to the transition radiation, and were measured by inserting a 0.127 mm-thick aluminum foil between the target and the detector[1,2].

Figure 2 shows the transition x-ray spectrum from a target consisting of eighteen 1 μm-thick beryllium foils for three different incident electron energies. The dots represent data from the experiment and the curve was calculated from a simplified theoretical description of transition radiation.[3] The agreement between experiment and theory is excellent and is typical of the results obtained with foils of the other materials mentioned above.

Figure 3 shows the energy-integrated transition x-ray angular distribution measured from the same beryllium target with an electron energy of 25 MeV. Again, the dots represent the data and the two solicd curves show theoretical predictions. The coherent prediction was calculated assuming that the transition radiation generated at the two surfaces of a foil were spatially coherent. This assumption yields a prediction that differs from the incoherent prediction, which was calculated by multiplying two times the distribution expected from a single surface. It is apparent that our measured distribution matches the prediction of the calculation that assumes coherence between the two surfaces. For the coherent form, interference effects give a narrower angular spread of emmision angles and an increased peak intensity. This interference behavior is somewhat unusual because the distance between the surfaces is about 10^5 times greater than the photon wavelengths of interest, and is possible because of the strong relativistic contraction that is characteristic of scattering by relativistic particles.

The single foil coherence motivated an attempt to observe interference between the individual foils in a target. Inter-foil inteference is not apparent in the data in Fig. 3 because the inter-foil spacing for this target (approximately 3000μm) results in an interference pattern with structure that is much smaller than the 1- mrad resolution of the detector.

Figure 4 shows angular distributions (Fig. 4(a) and 4(b)) and spectra (Fig. 4(c) and 4(d)) measured from two different targets exposed to a beam of 54 MeV electrons. Each target used two 0.55 μm-thick polypropylene foils; but one target had an inter-foil spacing of 3000μm, while the second had a 50-μm spacing. The differences between the two angular distributions are obvious. The oscillations in the angular distribution for the 50 μm-spaced target are caused by interference effects between the two foils. Again, the data (dots) is compared with corresponding predictions (solid curves). The sharp oscillations in the prediction for the 3000μm spacing were not resolvable by the detector But for the 50 μm spacing the interference oscillations are very broad in angle and the data and prediction agree remarkably well. In these cases, the actual source strengths are greater than the plots indicate because the detector efficiency (approximately 25%) was included in the calculations.

The spectra in Fig. 4(c) and 4(d) were recorded at the angles indicated on the corresponding angular distributions. The strong peak near 150 eV that dominates the spectra is associated with the polypropylene foil thickness. The spectrum in Fig. 4(c) is typical of spectra recorded over a wide range of emission angles for the 3000 μm-spaced target. As Fig 4(d) shows, the spectra recorded for the 50 μm-spaced target show wide variations, depending on the particular emission angle chosen.

The results in Fig. 4 demonstrate inteference effects with photons having wavelength of about 83 Å between foils having a separation of 50 μm. In this case, the inteference occurs in a structure that is nearly 10^4 times longer than the wavelength of interest. This behavior demonstrates that each transition photon is a coherent response to the entire target structure. This is true for our results because the experiments were always conducted with low average beam currents (below 10^{-10}A) where there was very rarely more than one photon at a time within the target.

In order to study these effects more carefully, we have performed energy-resolved measurements of the transition radiation angular distribution. Figure 5 shows the experimental arrangement for these measurements. A Si/W multilayer resonant reflector with a 2d period of 1479.2 Å and measuring 1" by 2.75" was placed in the beam line and used as the basis of a simple x-ray monochromator. Then the reflector was rotated to an appropriate Bragg angle and the detector was placed at the appropriate position to measure the reflected x-ray angular distribution.

Figure 6 shows angular distributions that were measured in this fashion. Figure 6(a) shows the measured (dots) angular distribution of 180 eV photons generated when 54 MeV traversed the same two-foil target with the nominal 50-μm spacing described previously. Unfortunately, in this case, the portion of the data file for emission angles less than 4 mrad have been lost, but the remainder of the data clearly shows the interference pattern that is characteristic of this particular situation. Figure shows similar data for a photon energy of 250 eV. The calculations (solid curves) show excellent qualitative agreement with the form of the measured patterns. In order to obtain the best possible comparison, the calculations have been multiplied by a normalization factor that corresponds to the reflectivity of the multilayer relector at the appropriate wavelength. We found that in order to achieve good agreement between the measured and calculated distributions, the foil thickness and separation had to be changed from their nominal values of 0.55 and 50 μm, respectively, to 0.60μm for the foil thickness and 60 Mm for the separation. This agreement could not be achieved for both energies by adjusting either the foil thickness of spacing alone.

The foil thickness had been measured by several different techniques, and the nominal value of 0.55 μm was only accurate to within ±10%. Thus, the thickness that was inferred from the calculations shown in Figure 6 is consistent with the possible range of foil thicknesses.

The foil separation had not been measured, but was inferred from the target assembly technique. The foils had been glued to the surface of one cm square silicon frames having a 7 mm square clear aperture. Thus, the 50-μm value was the minimum value that could have been expected from this structure. The inferred value of 63μm is consistent with the presence of a thin layer of glue that slightly increased the foil separation.

The calculations in Figure 6 have been used to infer the foil thickness and separation. In order to do this, the calculations assumed that the frequency-dependent dielectric constant, $\epsilon(\omega)$, of the polypropylene was given by the Drude free-electron approximation: $\epsilon(\omega)=1-(\omega_p/\omega)^2$, where ω_p is the plasma frequency of polypropylene and ω is the photon frequency. Now, if independent means can be used to characterize the target structure, then the analysis demonstrated above can be turned around and used to measure the frequency-dependent x-ray dielectric constant of the foil material: for each monochromator photon energy, ϵ could be determined.

Another application of our results might be the development of a tuneable, spatially coherent x-ray sourcee driven by 50 MeV electrons. In this case, the number of foils in the target would be increased and the transition photon energies would be determined by the emission angle. For a given angle of emission the photon energy, E, would be defined with a precision approximated by: $\Delta E/E=1/N$, where N is the number of foils in the target. However, the number of foils would be limited to give a total thickness not much larger than the x-ray absorption length for the photon energies of interest. Figure 7 shows a contour plot of transition photon energy vs. angle of emission. The contours show that the photon energies would vary in a predictable way with angle of emission

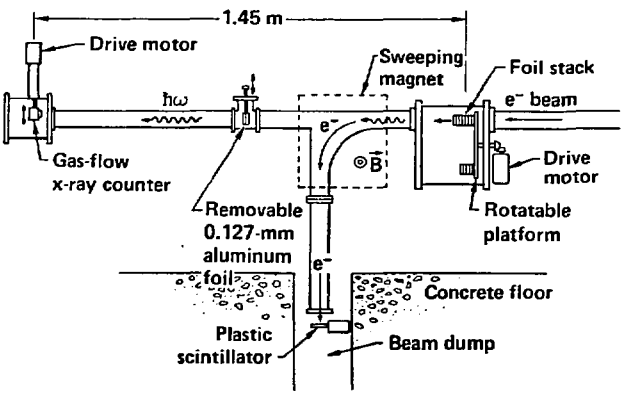
1.45 m
Drive motor
Sweeping magnet
Foil stack
e⁻ beam
ħω
e⁻
⊙B
Drive motor
Gas-flow x-ray counter
Removable 0.127-mm aluminum foil
Rotatable platform
e⁻
Concrete floor
Plastic scintillator
Beam dump

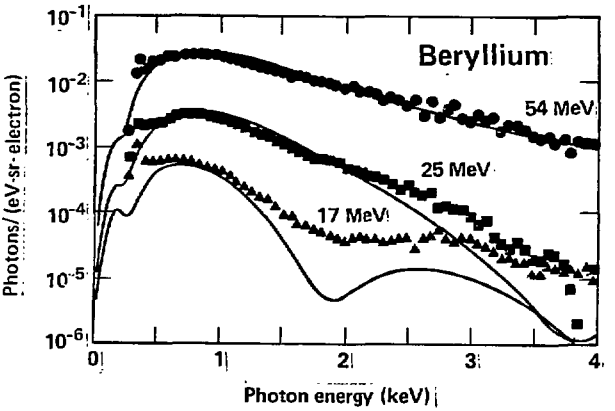
Beryllium
54 MeV
25 MeV
17 MeV
Photons/(eV·sr·electron)
Photon energy (keV)
10^{-1}
10^{-2}
10^{-3}
10^{-4}
10^{-5}
10^{-6}
0
1
2
3
4

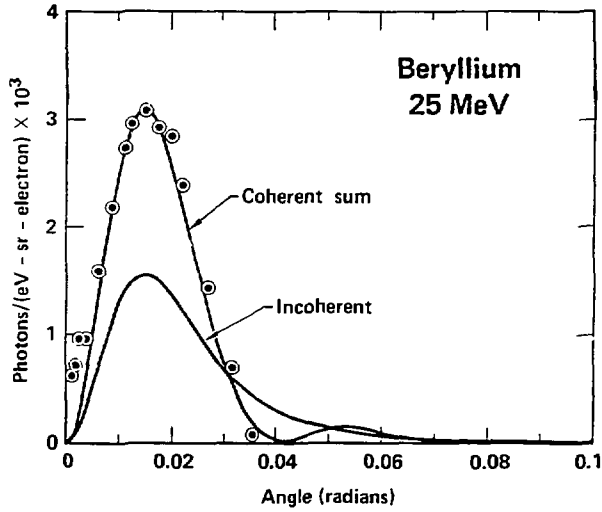
Beryllium
25 MeV
Coherent sum
Incoherent
Photons/(eV - sr - electron) X 10^-3
Angle (radians)
0
1
2
3
4
0
0.02
0.04
0.06
0.08
0.10

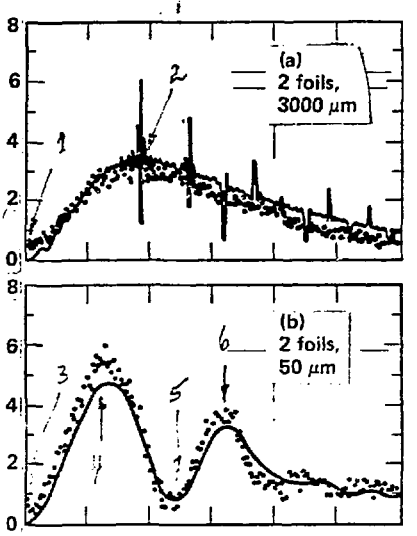
(a)
2 foils,
3000 μm
(b)
2 foils,
50 μm
1
2
3
4
5
6

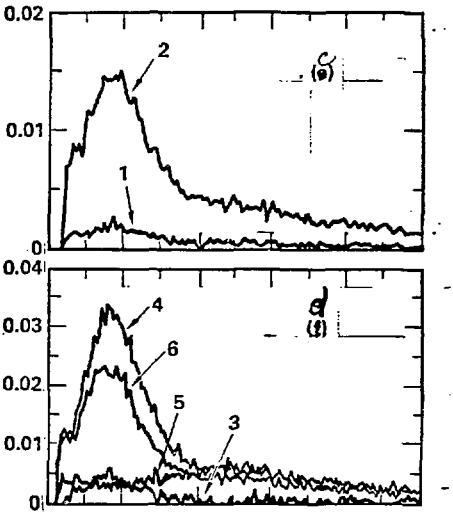
(e)
(f)
1
2
3
4
5
6

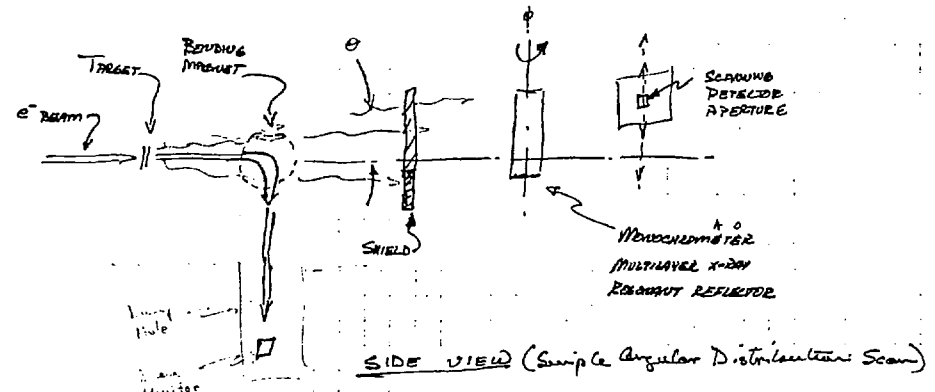

SIDE VIEW (Simple Angular Distribution Scan)

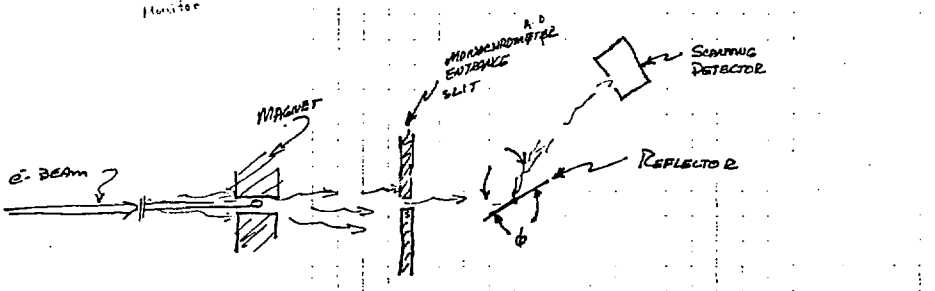

TOP VIEW (Monochromator Geometry)

Figure 5

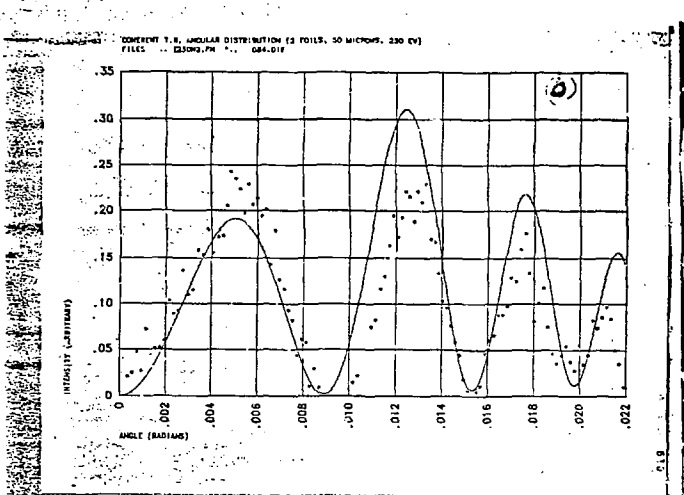
COHERENT T.R. ANGULAR DISTRIBUTION (2 FOILS, 50 MICRONS, 230 EV)
FILES .. [30M2.PH *.. 086.DIF
(a)
INTENSITY (ARBITRARY)
ANGLE (RADIANS)
.35
.30
.25
.20
.15
.10
.05
0
.002
.004
.006
.008
.010
.012
.014
.016
.018
.020
.022

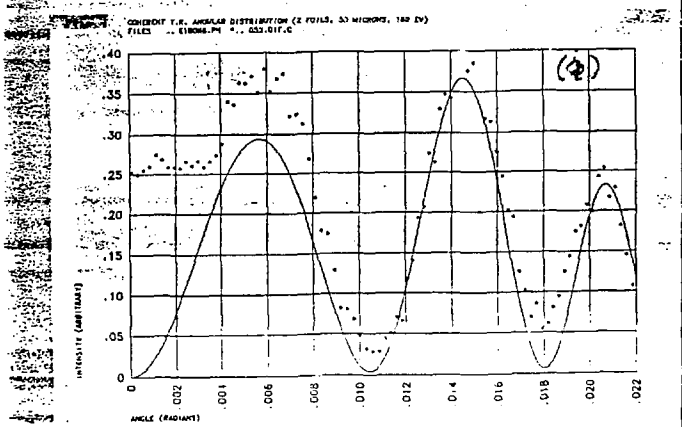
COHERENT T.R. ANGULAR DISTRIBUTION (2 FOILS, 53 MICRONS, 180 EV)
FILES .. [18M86.PH *.. 053.DIF.C
(b)
INTENSITY (ARBITRARY)
ANGLE (RADIANS)
.40
.35
.30
.25
.20
.15
.10
.05
0
.002
.004
.006
.008
.010
.012
.014
.016
.018
.020
.022

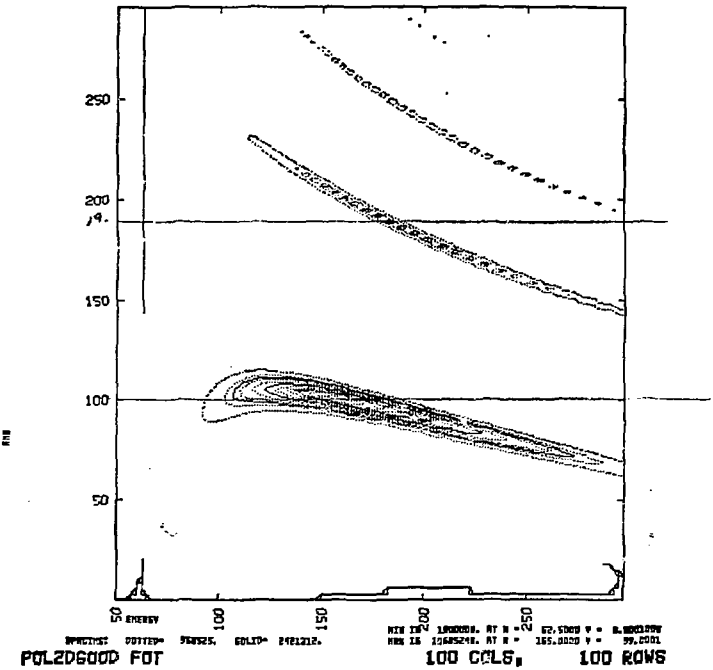
250
200
150
100
50
50
100
150
200
250
ENERGY
POL2D600D FOT
100 COLS
100 ROWS